TITLE: # Planck LFI 30/44 GHz Sky Load Implementation

DOC. TYPE: TECHNICAL NOTE

PROJECT REF.: PL-LFI-PST-TN-051 **PAGE:** 1 of V, 25

ISSUE / REV.: 1.0 **DATE:** March 12, 2004

Prepared by	**F. CUTTAIA** **L. TERENZI** **L. VALENZIANO** **LFI Project System Team**	**Date:** **Signature:**	March 12, 2004 _____
Agreed by	**C. BUTLER** **LFI** **Program Manager**	**Date:** **Signature:**	March 12, 2004 _____
Approved by	**N. MANDOLESI** **LFI** **Principal Investigator**	**Date:** **Signature:**	March 12, 2004 _____

DISTRIBUTION LIST

Recipient	Company / Institute		Sent
J. MARTI-CANALES	ESA – Noordwijk	Javier.Marti.Canales@esa.int	Yes
N. MANDOLESI	IASF – Sezione di Bologna	mandolesi@bo.iasf.cnr.it	Yes
C. BUTLER	IASF – Sezione di Bologna	butler@ bo.iasf.cnr.it	Yes
M. BERSANELLI	Unimi – Milano	Marco.Bersanelli@uni.mi.astro.it	Yes
B. COLLAUDIN	ALCATEL Space Ind.	Bernard.Collaudin@space.alcatel.fr	Yes
M. BALASINI	LABEN – Vimodrone	balasini.m@laben.it	Yes
F. MONZANI	LABEN – Vimodrone	fmonzani@webmail.laben.it	Yes
P. LEUTENEGGER	LABEN – Vimodrone	leutenegger.p@laben.it	Yes
P. GUZZI	LABEN – Vimodrone	guzzi.p@laben.it	Yes
A. MENNELLA	IASF – Sezione Milano	daniele@mi.iasf.cnr.it	Yes
L. VALENZIANO	IASF – Sezione di Bologna	valenziano@ bo.iasf.cnr.it	Yes
L. TERENZI	IASF – Sezione di Bologna	terenzi@bo.iasf.cnr.it	Yes
F.VILLA	IASF – Sezione di Bologna	villa@ bo.iasf.cnr.it	Yes
M.SANDRI	IASF – Sezione di Bologna	sandri@ bo.iasf.cnr.it	Yes
LFI System PCC	IASF – Bologna	lfispcc@bo.iasf.cnr.it	Yes

CHANGE RECORD

Issue	Date	Sheet	Description of Change	Release
0.1	Dec, 1st, '03	All	Draft issue of this document	
1.0	March,12th,'04	All	First Issue	IHDR

TABLE OF CONTENTS

LIST OF FIGURES

LIST OF TABLES

1 INTRODUCTION

1.1 Purpose

The LFI instrument is composed by 11 Radiometer Chain Assembly-RCA (6 at 70GHz, 3 at 44GHz, 2 at 30GHz). Each RCA is constituted by a Feed Horn, and Ortho Mode Transducer (OMT) a Front-End Module (FEM), containing the cold amplifier section, a complex Waveguide with links the Front –End to the Back-End Module, containing the warm amplifier section and the detectors.
Each RCA shall be calibrated before being mounted in the LFI Radiometer Array Assembly in a thermal and RF environment fully representative of flight conditions. Dedicated cryo facilities are built to fulfill these requirements.
One of the most critical items in calibration of the LFI radiometers is the Sky Simulator, also called Sky Load (SL). This object shall represent as close as possible the power emitted from the sky during Planck flight operation. Since the sky emission, at Planck frequencies, is dominated by the CMBR (an almost perfect blackbody at T=2.7K), the SL shall be an extremely good blackbody at the LFI frequencies. It shall be cooled to approximately 4K and shall be stable in temperature, as specified in the calibration document.
A SL for the 30 and 44GHz RCAs' calibration has been designed and modeled, both from the RF and the thermal point of view.

Purpose of this note is to characterise the behaviour of the calibrator named 'RCA SKY LOAD'(RCA-SL); the specific feature to investigate is the equivalent temperature seen by the feed. To do this, it needs both a radio-frequency and a thermal analysis, being the specific emissivity and the physical temperature of the load strictly tied. Only a combined unitary analysis can allow to maximise the radiometric emissivity and the thermal stability, taking into account radiometric fluctuations of the different parts arising from fluctuations of the reference temperature source.

1.2 Document overview

In Section 2, a description of the load design is given.
Section 3 reports the main requirements of a good microwave calibrator, from the radiometric point of view.
In Sections 4-6 details are reported about procedures and results of the RF study performed to define the design of the best system matching the requirements above.
Section 7 describes a thermal analysis of the system, implemented in a dedicated cryogenic environment.
In Section 8, we propose a combined RF and thermal study aimed to get an accurate characterization of our system, which is to be used as a calibrator of a high sensitivity instrument.

1.3 ACRONYMS

RCA-SL	Radiometer Chain Assembly – Sky Load
4K RL	4 Kelvin Reference Load
CMBR	Cosmic Microwave Background Radiation
TBC	To Be Confirmed
WG	Waveguides
RF	Radio Frequency
OMT	Ortho Mode Transducer
FEM	Front-End Module
RCA	Radiometer Chain Assembly
RAA	Radiometer Array Assembly
CMBR	Cosmic Microwave Background Radiation

2 Design

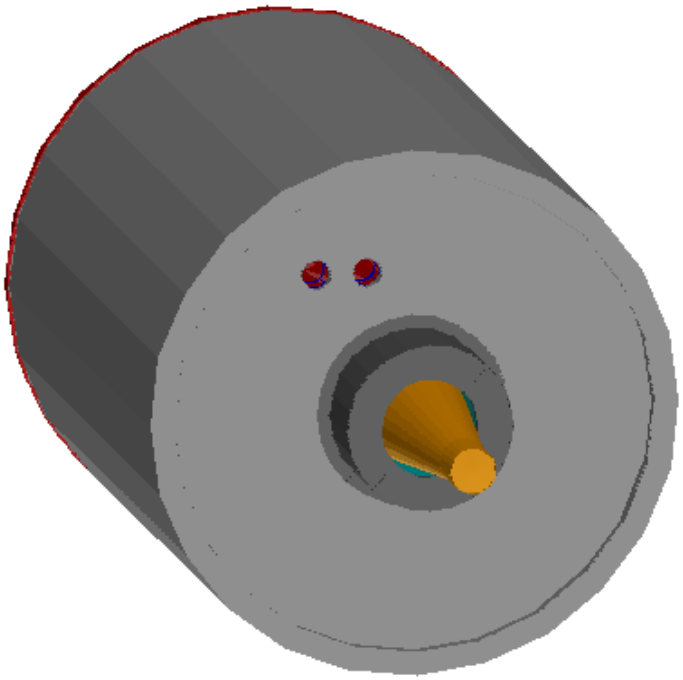

Figure 1 SKY LOAD 3D rendered representation. Are shown: the FEED HORN(orange), the LID (gray) with two holes to lodge two waveguides, the LID ADAPTOR METAL SHIELD (dark gray) allowing to lodge the two feed horns with different size at 30 GHz and 44 GHz, the external metal CYLINDER SHIELD.

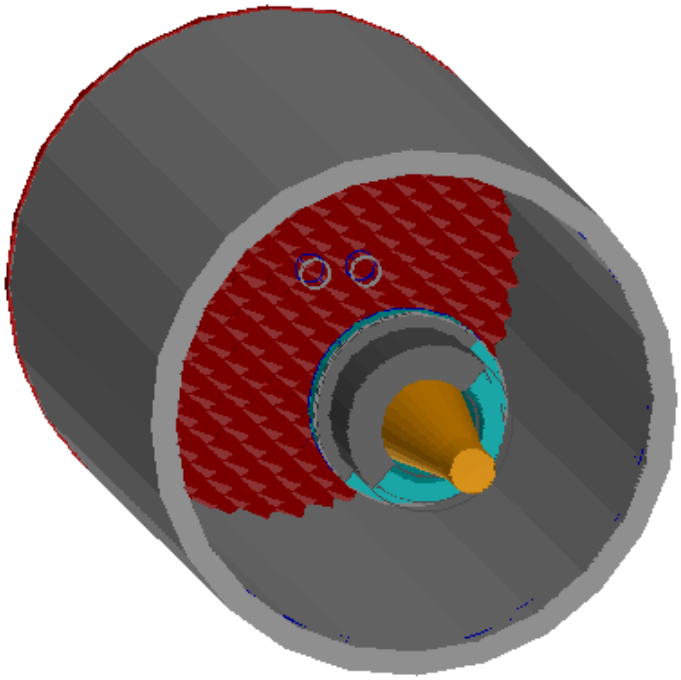

Figure 2 SKY LOAD rendered-wireframe mixed representation. Are shown: the FEED HORN(orange), the LID ADAPTOR METAL SHIELD (dark gray), the LID ABSORBING ADAPTOR (light blue), the ABSOBING WALLS (gray), the BASE (bed of pyramids, red)

The RCA-SL is, in its last configuration (see Figure 1 and Figure 2), designed in order to observe mechanical constraints and radiometric requirements (§3). We assume a cylindrical symmetry around an axis coincident with the feed horn's symmetry axis.

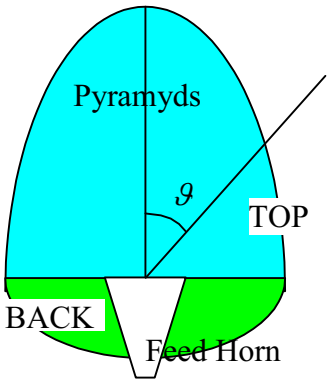

Figure 3: Sketch of the geometrical regions used in the analysis. Cylindrical symmetry around the Feed Horn axis is assumed (i.e. definitions independent from the azimuth angle). Region called TOP, in front of the Feed Horn, is sketched in light Blue. Region behind the Feed Horn, called BACK, is colored in light green.

The volume of the SL can be logically separated in two geometrical regions, defined by the zenith angle θ: the first one (that from now on it will be named 'TOP'), located in front of the feed, having its mouth co-planar with the feed aperture ($\vartheta \leq 90°$, for any azimuth angle) depicted in light blue; the second one (that from now on it will be named 'BACK'), surrounding the feed without touching it, for $90° < \vartheta \leq 180°$, depicted in light green. The TOP region contains an empty absorbing cylinder (called 'WALL'. with thickness of 10mm) having length (L) of 270mm and external diameter (D) of 220mm, open in the side facing the feed, closed in the opposite side by means of a circular base (that from now on will be named 'BASE') 10mm tick, holding a network of pyramids having tips turned towards the feed. Pyramids have a height of 30mm and square base with side of 5mm; they fill the whole circular area.

The BACK regions contains an annular lid (from now on it will be named 'LID') close to be co-planar with the feed's mouth. The LID has a coaxial hole of 40mm diameter, allowing to lodge two adaptors (LID ADAPTOR) of different size. This solution was implemented to allow a quick mounting of the two horns at 30 GHz and 44 GHz, having different mouth's size, and to preserve them from the radiation otherwise directly leaking inside the calibrator. The feed horn is mechanically, and so thermally, disconnected from the calibrator.

BASE, WALL, LID and LID ADAPTER are coaxial with the feed. These parts are made of absorbing material, bonded on a metallic enclosure (that from now on will be named 'COVER') 3mm thick; the CYLINDER must be perfectly joined to the BASE and the LID, for preserving both the electric and the thermal continuity. The material employed for all the absorbing parts is ECCOSORB CR110 (REF[4], REF[3], REF[5]). The dimensions of the WALL, BASE and COVER are summarised in Figure 4.

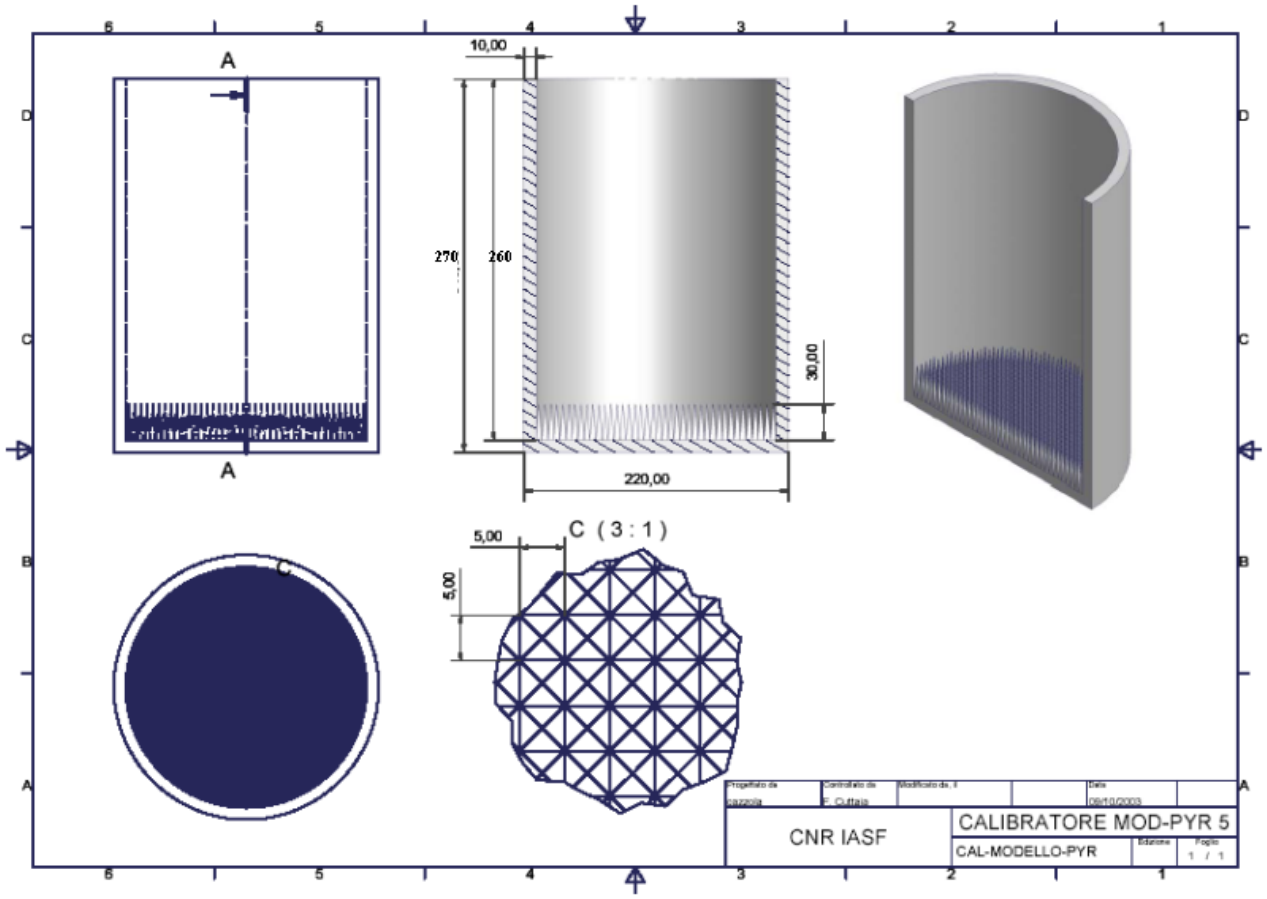

Figure 4 Pictorial view of the RCA-SL TOP part; The BASE covered with pyramids is also represented. The metal shield 3mm thick covering the RCA-SL is not shown.

2.1 Implementation inside the cryo-facility

The RCA-SL must be connected to a reference temperature source; the thermal link is made with the metal cylinder shield (COVER) bonded (using ECCOSORB CR110 as adhesive) to the absorbing cylinder. High thermal conductivity Aluminium was selected for the COVER, in order to increase the thermal homogeneity inside the load. However, this choice has as counterpart that a temperature fluctuation of the reference source propagates quickly inside the load. This thermal effect is investigated in §7

3 Requirements

The RCA-SL must behave as a black body, characterised for having emissivity very close to one. The measurable quantity, useful to represent this characteristic, is the Return Loss (RL) , that is the fraction of the power outgoing the feed coming back trough the feed itself and detected by the receiver. The power emitted by the feed can be normalised to unit: in this way the RL can be expressed as a number ranging from 0 (null reflection) to 1 (full reflection), or, as is the habit, as ten

times the decimal logarithm of this quantity. The emissivity is strictly tied to the RL by the conservation energy law:

EQ[1] $P_{INCIDENT}=P_{REFLECTED}+P_{ABSORBED}+P_{TRANSMITTED}$

being in this case:

EQ[2] $P_{TRANSMITTED}=0$

and by applying the Kirchoff's law:

EQ[3] $$E_T = \int_0^\infty A_{\nu,T}\varepsilon_{\nu,T}d\nu$$

that expresses the integral emitting power E_T of a body (at a given temperature T) in function of its absorbing power $A_{\nu,T}$; for a black body, by definition, $\frac{E_T}{A_{\nu,T}} = \varepsilon_{\nu,T} = 1$; we can test the emitting characteristics by radiating the RCA-SL with a radiation ($P_{INCIDENT}$) and evaluating the absorption $A_{\nu,T} = 1 - P_{refl}$ by means of a measure of reflected power.

Then:

EQ[4] $P_{ABSORBED}=P_{EMITTED}$

The requirement of being a black body is required to avoid due to the two following undesirable effects:

- A body with emissivity lower than one does not have spectral characteristics of black body: since the Cosmic Microwave Background Radiation has a perfect black body spectrum, the signal to be compared with must have similar characteristics. The CMBR temperature is known with a precision of 1%; so, to obtain an accurate calibration, we need a RCA-SL having an emissivity higher than 99%. An acceptable margin leads to a requirement of a RL higher (in absolute value) than -25dB (emissivity higher than 0,9968).
- The second reason for a high emissivity, less important than the first one but however to be considered, is due to the noise power broadcasted by the radiometers through the feed horn. It is typically comparable to the radiometer's noise temperature. It varies depending on the channel and ranges from 8K(TBC) to 15K (TBC). This power is reflected, in the same wave band, by a non perfectly absorbing RCA-SL , and it sums to the black body power detected by the receiver. The effect is that to increase the reference temperature, degrading the radiometers performances that depend strictly on the 1/f behaviour (REF[8]) inversely to the temperature difference T_{sky}-T_{load}.

4 RF Model Description

A model-analysis for the RCA-SL must proceed in two directions: the feed horn characterisation and the SKY LOAD characterisation. In fact, whichever analysis cannot neglect the way in which the feed perceives the emission coming from different parts of the load. Moreover, a so done analysis will return useful when considering the weight of temperature fluctuations of individual parts of the load.

The RCA-SL model can be divided into three parts described in §2: the BASE (bed of pyramids backed by an absorbing cylinder 10 mm thick), the flat walls of the cylinder (WALL) and the LID.

The model evaluates the feed characteristics (by means of software GRASP 8) and the absorber characteristics (using the Finite Elements Method to compute the reflectivity of the BASE) by simulation; the emissivity of the WALL and LID and the improving in emissivity due to the multiple reflections inside the cylinder are evaluated analytically. In this aim, the three features described in the next paragraphs have to be accurately considered.

4.1 The near field pattern

The near field pattern should be evaluated as a normalized pattern depending on the radius and on the angle. For each angle θ, the distance r of the phase centre of the feed from the point obtained as intersection with the RCA-SL surface is calculated. For each distance r, the near field pattern is evaluated and is computed the power as a function POWER(r, θ). The power emitted in each angle is normalized to the total power emitted over the full solid angle, putting this latter equal to unit.

$$\text{EQ[5]} \quad \sum_{r,\vartheta} Power(r,\vartheta) = 1$$

As a preliminary estimation, [POWER(r,θ)] has been approximated by $[POWER(\theta)]_r$, that is the power pattern evaluated over a sphere of radius r = L, where L is the distance between the feed phase centre and the ideal plane passing trough the pyramids' tips.
We outline some general rules describing the near field behaviour.

The near field pattern directivity increases with distance, approximating the Far field pattern as r approach the Far field length (approximately $2\pi \cdot D^2/\lambda$): it means that the main power is emitted under a narrower solid angle.

Discrepancies between two near field patterns become less appreciable approaching the far field radius.

4.2 The intrinsic body emissivity ε

Each part of the load has a different emissivity depending on various parameters. The most important are listed below.

a) Electromagnetic parameters (fixed for each frequency): they rule over the absorption and reflection laws
b) Material thickness (absorption increases with thickness, reflection keeps almost constant behind a certain characteristic thickness)
c) Incidence angle (changes the crossed thickness).

d) Geometry (the worst case is that of a flat surface, the best case that of a perfectly matched surface; in the specific case of this work, a pyramid is a geometry tapering the impedance to the incoming radiation) (REF[6] §6).
e) Surface machining (ruling on the reflectance and on the diffusivity: it strictly depends on the wavelength)

4.3 The cavity effect

It is due to the multiple reflections inside the cavity: it is directly proportional to the number of interactions (reflections and absorptions) inside the cavity, before the radiation reaches the detector. It is tightly related (direct proportional) to:

a) Ratio L/D
b) Ratio R_2/R_1

With R_2=D/2 and R_1 being the internal radius of the LID.
For a cylinder, the cavity contribute to the total emissivity can be separated into three individual contributes, coming from:

a) The bottom surface (BASE)
b) The Cylinder surface (WALL)
c) The annular lid (LID) closing the gap between the walls and the source: the assumption that the internal radius of the lid coincides with the source radius has been made In the real case a little gap material exists between them.

Once the properties at point 4.2 are fixed, it can be stated that:

a) The effective emissivity of the emitting surfaces grows with L/D (with different weights and behaviours depending on the specific part); in fact the number of reflection inside the cylinder increases.
b) The effective emissivity grows with R_2/R_1 ; in fact the detector sees an absorbing surrounding with increasing size respect to the size of its collecting area.

5 Evaluation of the total effective emissivity

5.1 Power emitted

The contribute to the total effective emissivity can be computed as:

EQ[6] $$\varepsilon_{eff} = P_B \cdot C_B(\varepsilon_B) + P_W \cdot C_W(\varepsilon_W) + P_L \cdot C_L(\varepsilon_L)$$

where:

a) P_i is the normalized near field power received (reciprocity theorem) from the feed under the solid angle subtended respectively by the BASE, the WALL, the LID.
b) ε_i is the intrinsic emissivity of each part.
c) C_i is the contribute to the cavity effect given by each part.

If $\varepsilon_B = \varepsilon_W = \varepsilon_L$ (a cylinder with BASE, WALL and LID made of the same material, with the same thickness, machined with the same shape), then ε_{eff} grows always with the simultaneous growing of the ratios L/D and R_2/R_1;
If, however, as it is our situation, the three parts have different characteristics (i.e. they have different emissivity ε_i), it is not possible to define homogeneously the behaviour of the entire SL. In fact, as r grows, the solid angle subtended by each part changes, changing the relative weight of each part of the SL. This fact excludes the possibility of considering the Black Body emission as a feature of the cylinder alone, independently on the source characteristics (especially operating frequency and directivity).
In our case, the absorbing characteristics are maximum for the BASE, because of its shape as pyramidal network: a compromise has therefore to be found in setting the right L (subtending an angle ϑ, varying inversely to L), to take into account both the directivity and the cavity effect C_B increasing with L, and the power emitted (absorbed) by the base, increasing with ϑ).

From the near field normalized power the three contributes P_i have been estimated (with the approximation described in the point 4.1). The normalization is referred to the total power emitted by the source into a 4π radians angle. Given the angles ϑ_B (subtended by the BASE $\vartheta_B = 23{,}5$ deg) and ϑ_L (subtended by the LID, that, supposed to be coplanar with the source's aperture, gives $\vartheta_L = \pi/2$ radians), and supposing that radiation cannot escape (leakage) out of the RCA-SL, the total power emitted from the feed can be written as:

EQ[7] $$P_{tot} = P_B + P_W + P_L = 4\pi[P(0 \le \vartheta \le \vartheta_L)\sin\vartheta\, d\vartheta + P(\vartheta_L < \vartheta \le \pi/2)\sin\vartheta\, d\vartheta + P(\pi/2 < \vartheta \le \pi)\sin\vartheta\, d\vartheta]$$

P_B/P_{tot}, P_W/P_{tot}, P_L/P_{tot} have been evaluated for L=230mm. The plots and the summarized results are displayed in Figure 5 ,Figure 6 and in Tab. 1, Tab. 2.

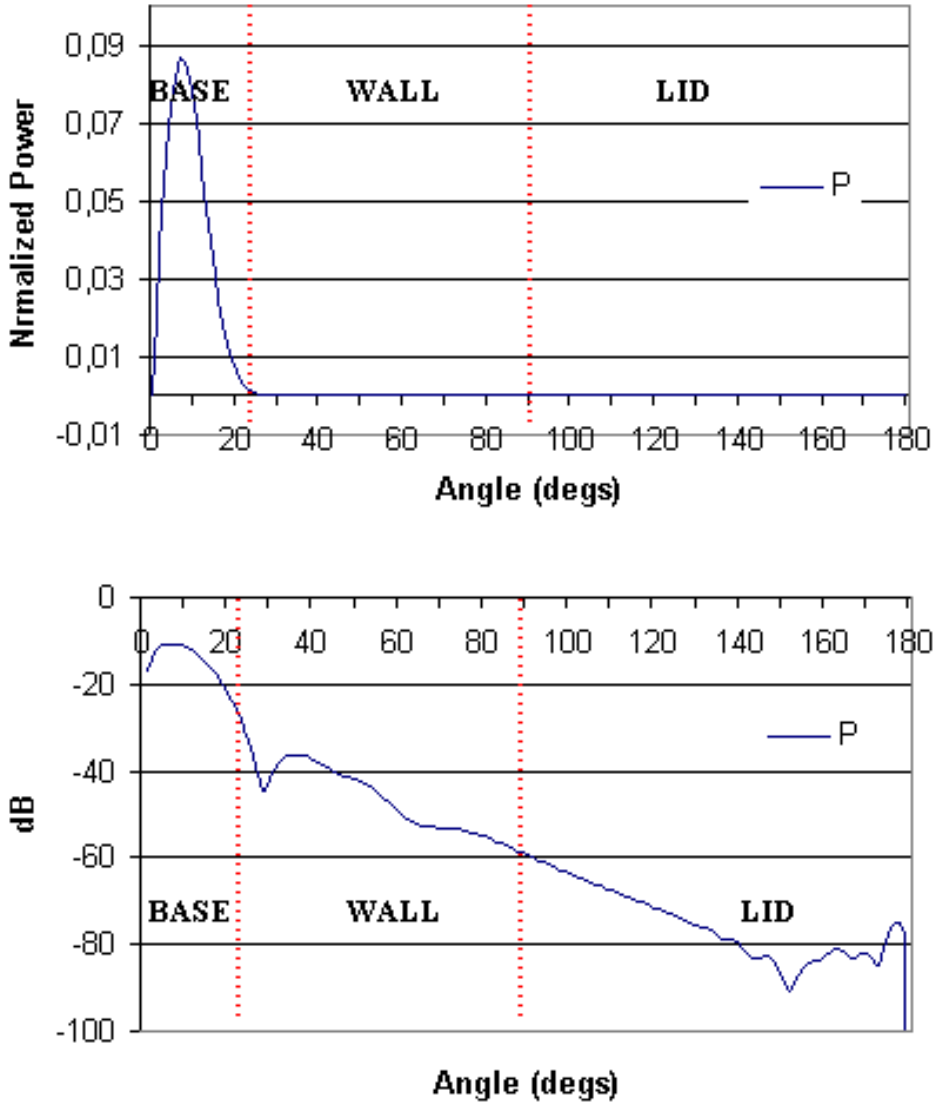

Figure 5 near field power distribution , evaluated at 30GHz, in the three parts BASE, WALL, LID, individuated by the dashed lines; values are normalised to the total power emitted by the feed. Both linear (top) and logarithmic (bottom) behaviours are reported.

	ϑ	P
BASE	23.5	0,9956
WALLS	90	0,00432
LID	180	1,17E-05

Tab. 1 Summary of the near field power distribution, evaluated at 30GHz, in the three parts BASE, WALL, LID. Is supposed $P_{tot} = 1$

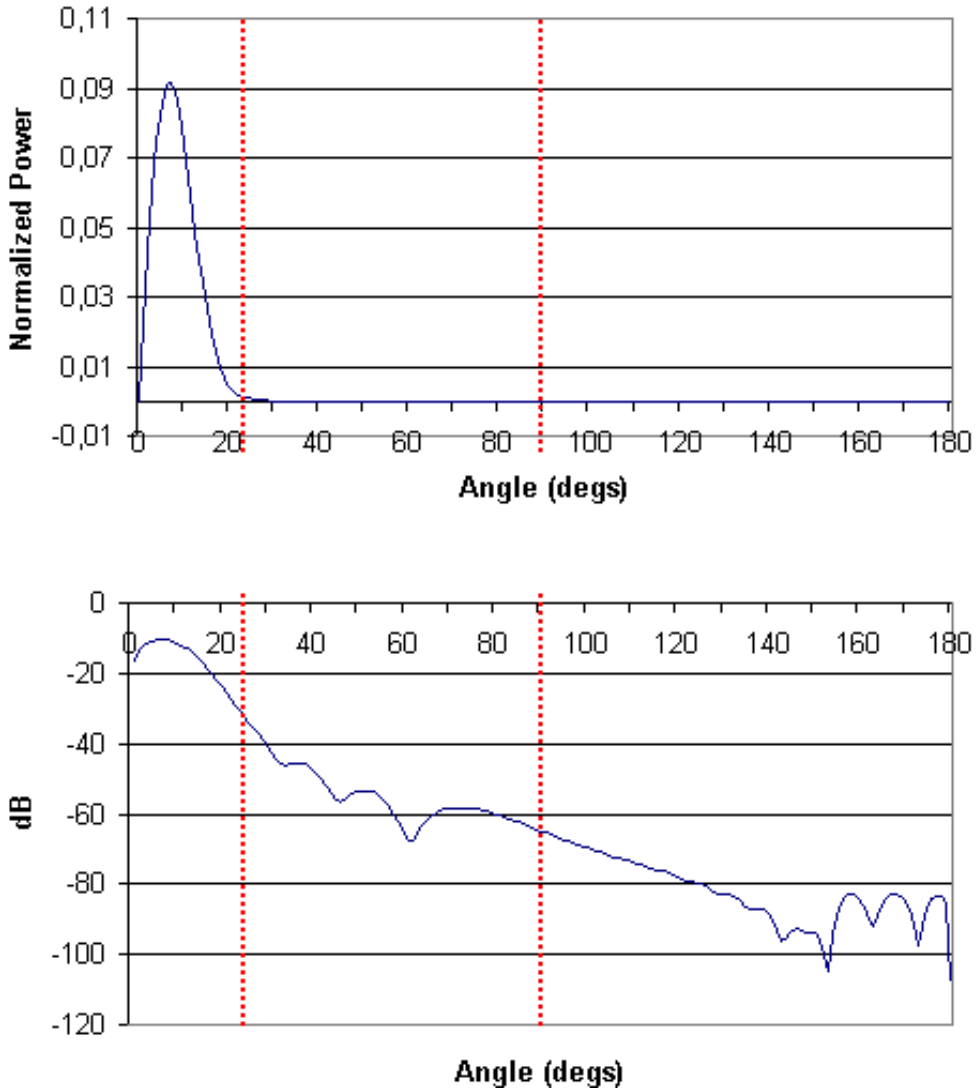

Figure 6 near field power distribution , evaluated at 44GHz, in the three parts BASE, WALL, LID, individuated by the dashed lines; values are normalised to the total power emitted by the feed. Both linear (top) and logarithmic (bottom) behaviours are reported.

	ϑ	P
BASE	23.5	0,9979
WALLS	90	0,00209
LID	180	2,41E-06

Tab. 2 Summary of the near field power distribution, evaluated at 44GHz, in the three parts BASE, WALL, LID. Is supposed $P_{tot} = 1$

As we observe from the two tables above, the most power is emitted into the solid angle subtended by the BASE and only an infinitesimal part are intercepted by the LID. The important function of

the LID, although it does not contribute if not minimally to the total emission, is to increase the emitting properties of the BASE and of the WALL, avoiding the radiation to escape the RCA-SL and increasing the number of reflections inside the full structure, before the radiation reaches the detector.

The behaviour does not significantly change with frequency passing from 30GHz to 44GHz, although a little increasing in the power intercepted by the BASE is registered in the latter case (it is explainable considering that the near field zone is closer for smaller wavelengths).

5.2 Evaluation of the coefficients C_i

They could be obtained by means of an iterative procedure taking into account a geometrical ray tracing of n-order (the maximum order is set with some convergence criterion) and the absorption properties (ε_i components). However, at this level of the analysis, we try only to make a worst case prediction, basing on studies from literature describing the emissivity of cylindrical diffuse cavities in terms of their geometry (REF[1], REF[2])
This studies have some limits:

a) They consider all surfaces as having the same effective emissivity.
b) The individual behaviour are, at present, available only for discrete values of ε_i .
c) They do not take into account the wavelength (diffusivity must be referred to some wavelength).

Due to the cavity effect dependency on the effective body emissivity, we must characterise, at first, the three parts constituting the RCA-SL. We evaluated the effective emissivity of the BASE using a FEM method (REF[10]): it is about 0,999, with little variations depending on its relative extension respect to the detector size and on the frequency (electromagnetic parameters vary with frequency). Anyway we can assume a constant case with $\varepsilon_B = 0{,}999$.
The emission properties of the WALL and of the LID can be estimated analytically, representing them by a flat slab 10mm thick, metal backed. The incidence is supposed to be normal to the surface; the evaluation gives $\varepsilon_W = \varepsilon_L \sim 0{,}7$
We considered the analytical curve, obtained from (REF[1]), for a cylinder with L/D= 1 (in our case is L/D = 1,15) having the same intrinsic emissivity for the three parts: $\varepsilon_B = \varepsilon_W = \varepsilon_L = 0{,}7$.
The behaviour varies with the part considered and with its specific emitting zone. A non dimensional parameter can be assigned to each part, running over the length, expressed by the three ratios: *r / R2* (equal to unit for $\vartheta = \vartheta_B$), *x/ L* (equal to unit for $\vartheta = \vartheta_W$), *z/ (R1-R2)* (equal to unit for $\vartheta = \vartheta_L$).

The curves following represent the Ci coefficients with respect to the above parameters.

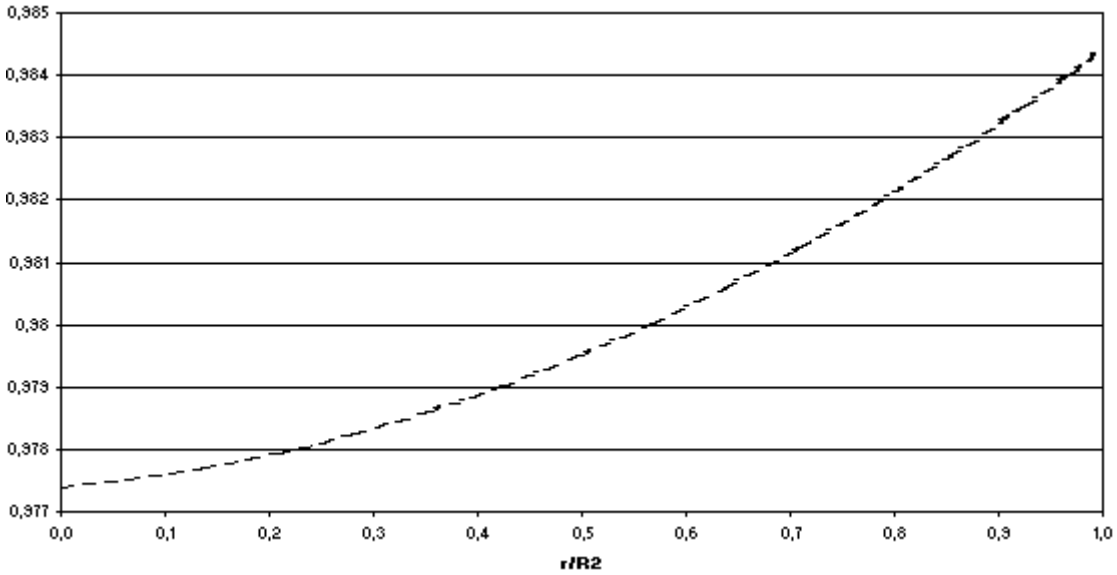

Figure 7 C_B coefficient curve: on the x axis is r/R_2, on the y axis C_B

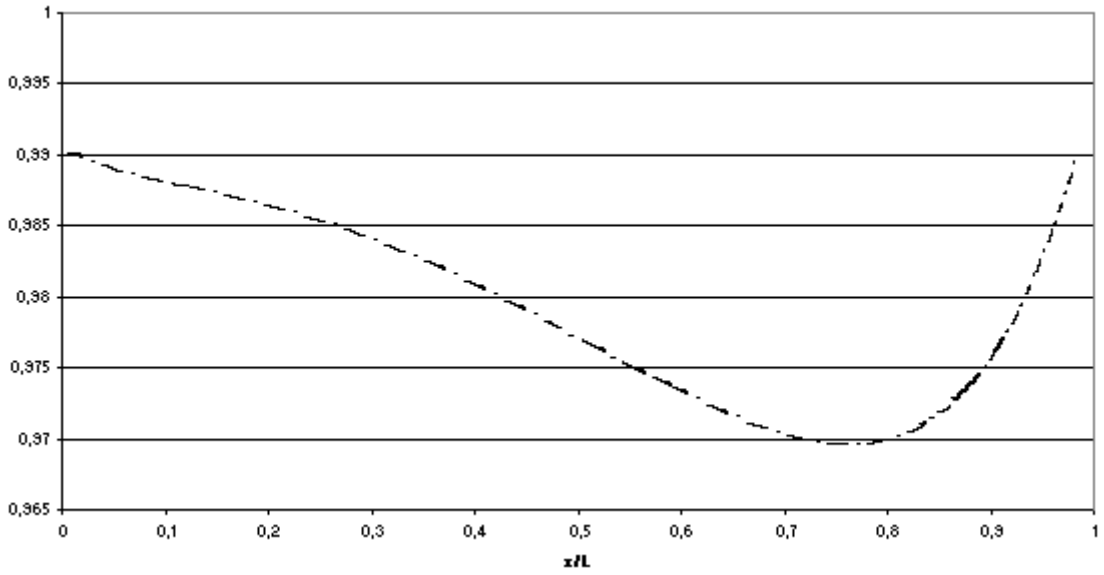

Figure 8 C_W coefficient curve: on the x axis is x/L, on the y axis C_W

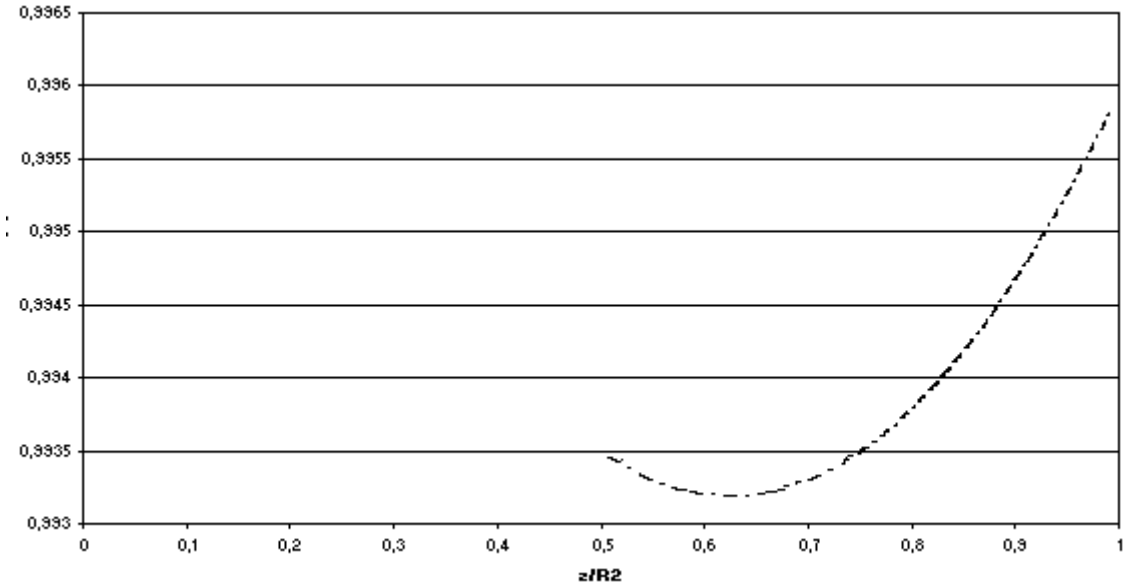

Figure 9 C_L coefficient (the curve is evaluated for a detector with collecting area one half the base radius; the plot ranges from 0,5 to 1 in units of z/R2 because the length ranging from 0 to 0,5 is occupied by the feed's mouth)

By observing the three plots above representing the C_i, it is possible to state that:

a) The cavity effect increases strongly the effective emissivity of the single components (making it grow from 0,7 to more than 0,97 for all the cases).
b) The cavity effect has a strong dependency on the spatial distribution. Its worst performances are especially registered in the part WALL, approaching the mouth.

6 Data analysis

As said above, the three coefficients are computed for bodies with intrinsic emissivity ε =0,7. However, while for the WALL and the LID it can be considered as a realistic case, for the BASE the input parameter ε_B is largely underestimated; the comparison of graphs computed at different values of ε_B (REF[1]) shows that C_B increases faster than ε_B . In our case, the starting point is $C_B(\varepsilon_B=0.999)$, so it seems realistic to assume C_B at least the same order of the contribute ε_B given to the total emissivity by the BASE. This behaviour is assumed to be constant over the whole BASE. So we will state C_B=0,999

EQ[8] $[P_B * C_B]_{30GHz} = 0.9946$
EQ[9] $[P_L * C_B]_{44GHz} = 0.9969$

We can multiply the P_i and C_i components (relative to the WALL) only after expressing both them respect to the same parameter ϑ; then we get a normalised integrated emissivity pattern by summing the terms $[Pi(\vartheta)*C_i(\vartheta)]_B$ over the whole range $\vartheta_{[BW]}$ (comprised between $\vartheta_B = 23,5°$ and $\vartheta_W = 90°$).

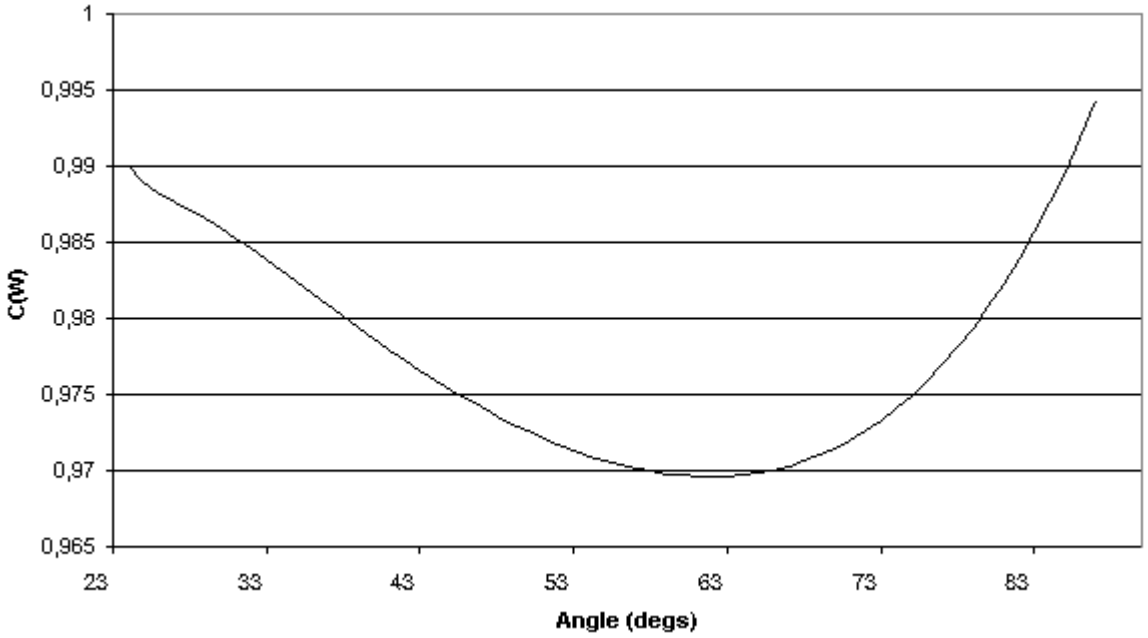

Figure 10 C_W coefficient expressed in function of the angle subtended by the WALL respect to the phase center of the detector

For what concern the C_L contribute to the total emissivity, it has been considered that the LID provides only a minimum contribute to the power detected (see Tab. 1 and Tab. 2); so, instead of multiplying $[Pi(\vartheta)*Ci(\vartheta)]_L$ for each component, it suffices to evaluate the average $\underline{C_L}$ (that is 0,9942) and to multiply it times the total power P_L. This operation gives:

EQ[10] $[P_L * \underline{C}_L]_{30GHz} = 1.14\ E\text{-}05$
EQ[11] $[P_L * \underline{C}_L]_{44GHz} = 2.38\ E\text{-}06$

Instead, by multiplying the curve in Figure 10 times the behaviours (in the range defined by the two red dashed lines) in Figure 5 and Figure 6 , and integrating over the whole range, it has been obtained:

EQ[12] $$\left[\int_{\vartheta_L}^{\pi/2} P_W(\vartheta)\cdot C_W(\vartheta)\cdot d\vartheta\right]_{30GHz} = 0.00429$$

EQ[13] $$\left[\int_{\vartheta_L}^{\pi/2} P_W(\vartheta)\cdot C_W(\vartheta)\cdot d\vartheta\right]_{44GHz} = 0.00207$$

By combining respectively EQ[8], EQ[10], EQ[12] and EQ[9], EQ[11], EQ[13] we find the searched result for the total emissivity perceived by the feed at the two frequencies 30GHz and 44 GHz:

EQ[14] $[\varepsilon_{TOT}]_{30GHz} = 0.99890$
EQ[15] $[\varepsilon_{TOT}]_{44GHz} = 0.99897$

That is, for the two reflectivity (expressed in logarithmic form):

EQ[16] $[RL]_{30GHz} = -29.5$ dB
EQ[17] $[RL]_{44GHz} = -29.6$ dB

In principle, assumed to be realistic the analytic model giving the coefficients C_i, the values found should represent two worst cases. A more accurate analysis will be performed in the next feature taking into account:

a) The cavity effect evaluation for the exact ratio L/D
b) The improving effect of the increased specific emissivity ε_B (respect to the model considered here, having $\varepsilon_B=\varepsilon_W=\varepsilon_L$) produces a C_W and C_L improvement; a more accurate analysis would evaluate C_W and C_L as functions of ε_B.
c) The Eccosorb electro-magnetic behaviour at 4°K. Electric tangent loss and permeattivity employed in the FEM model have been evaluated only at room temperature (REF[7]).
d)

7 Thermal analysis

A thermal study of the calibrator design was developed, in order to evaluate the impact of thermal fluctuations level in different regions of the cylinder, caused by cooler instabilities.

7.1 Thermal Model

A thermal model of the system was built (Figure 11), taking into account geometrical design and thermal properties of the structure materials.

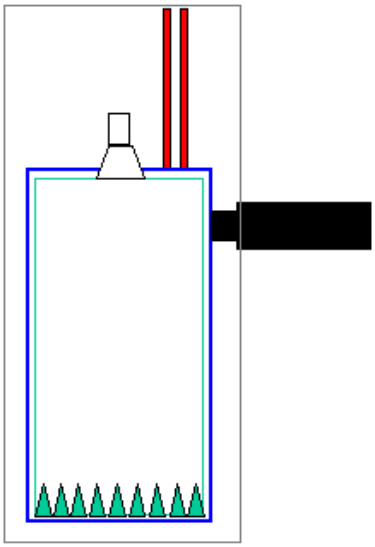

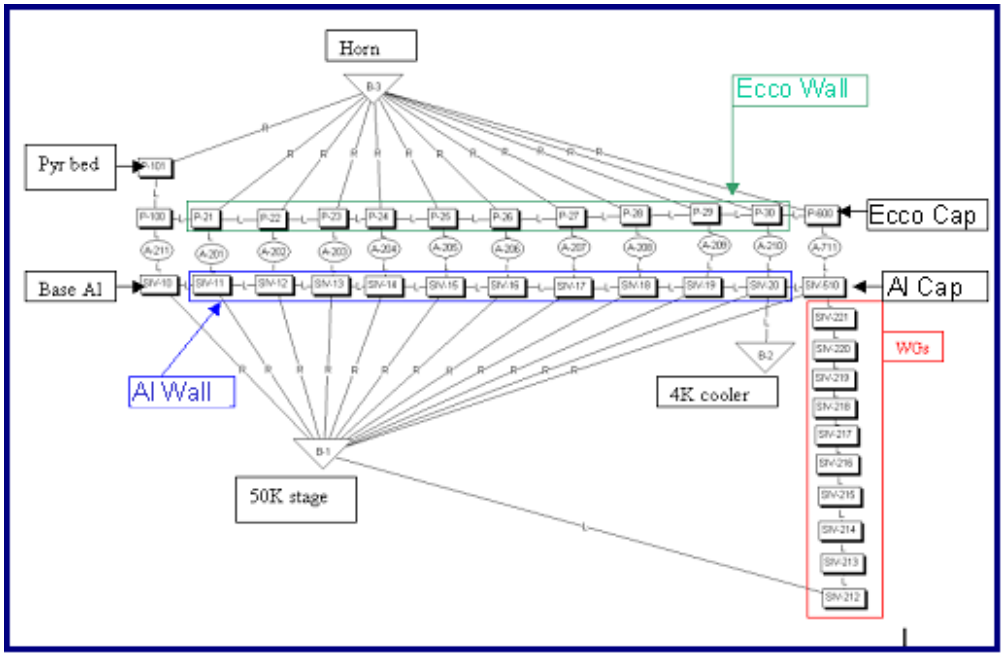

Figure 11 Thermal scheme of the cold load in the cryo-facility(left) and nodes setup for thermal analysis (right). B2 is the cooler boundary node (black in the left figure), B1 is the 50 K shroud (light grey), P101 is the pyramid bed, nodes 11-20 represent the aluminium envelope (blue), while nodes 21-30 represent the internal Eccosorb coating (green) and nodes 212-221 are for the stainless steel waveguides (red).

In this first model, the pyramids bed and the Aluminum base are treated as a whole, because we were interested in their general behavior. The 4K cooler interface is located in the upper side of the load, which is a choice due to dimensions of the cryo-chamber. We will show that, also from the thermal stability point of view, this setup is better than a scheme with the load located vertically upon the cooler cold head, whose fluctuations would affect directly the Aluminum base. Radiative loads upon the cold load, coming from the 50 K shroud and the 20 K horn are considered (R labeled links in the figure). Stainless steel waveguides connect 50 K stage to the 4K calibrator, through a path 30 cm long. Main thermo-physical properties used in the model are reported in the Tab. 3.

Al density	2713 Kg/m^3
Al thermal conductivity	5.148 W/m K
Al specific heat	0.218 J/Kg K
Al emissivity	0.02
Eccosorb CR110 density	1600 Kg/m^3
Eccosorb CR110 thermal conductivity (REF[9])	0.08 W/m K
Eccosorb CR110 specific heat (REF[9])	9.6 J/Kg K
Eccosorb CR110 emissivity	1.0
Stainless steel density	8050 Kg/m^3
Stainless steel thermal conductivity (4 K)	0.284 W/m K
Stainless steel specific heat (4 K)	1.9940 J/Kg K

Tab. 3 Thermal and physical properties used in the thermal model. All properties refer to the temperature of 4 K, but, for the stainless steel 316, the complete temperature dependence was considered in the simulations[1].

[1] Data available at the Cryogenic department of National Institute for Standards and Technology web page (http://cryogenics.nist.gov/NewFiles/material_properties.html)

7.2 Absolute Temperature and Wave Guides Impact

A first set of simulations was run, considering the 4K cooler, oscillating with a period of 60 s and an amplitude of 0.1 K, linked to the Aluminum base (Figure 12 left) and to the upper side of the load (Figure 12 right).

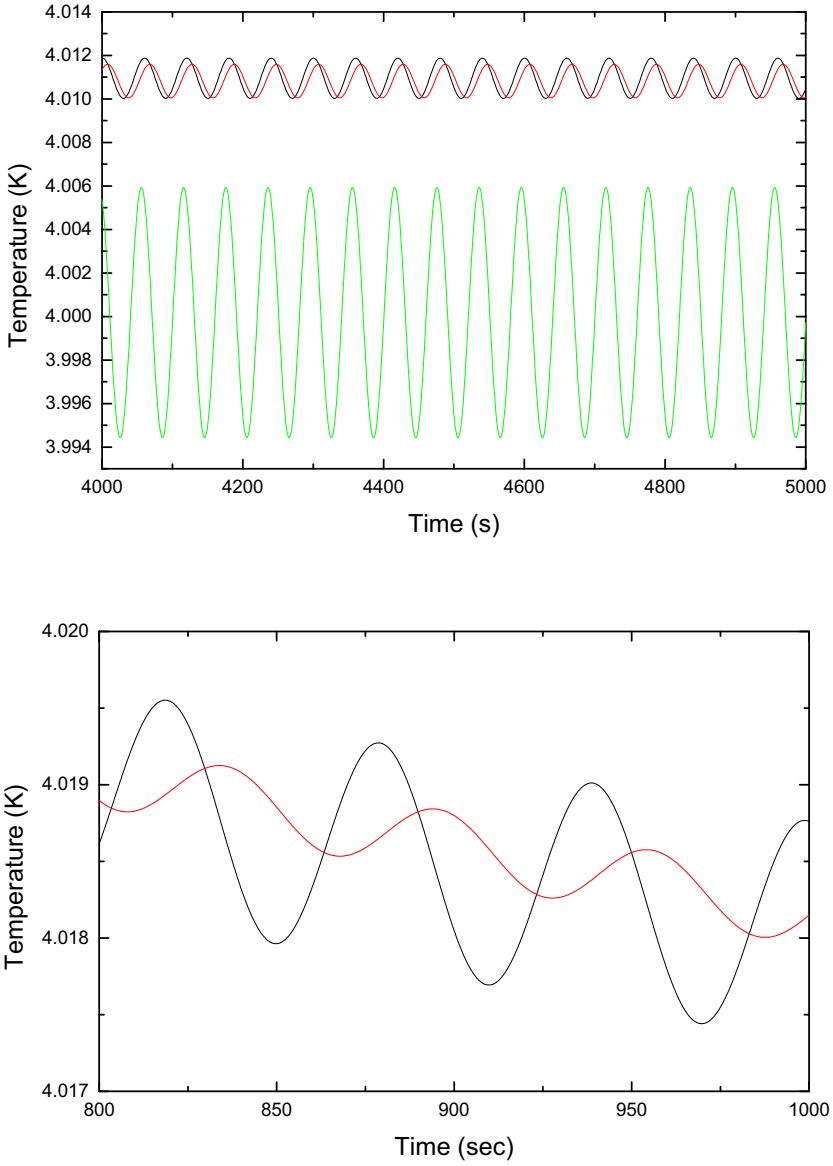

Figure 12 Temperature fluctuations at pyramid bed in the case of the 4K cooler linked to the load base (green curve in the left panel) and the case of the 4K cooler linked to the upper side of the load (red curve in the right panel).

From this analysis, we can see that fluctuations of the load base are damped in the current cooler interface configuration about a factor 10 with respect to the vertical one, while the absolute temperature will not grow too much (about 15 mK) with respect to the cooler one.

A second analysis was performed to check the thermal impact of waveguides, connecting the 50 K shroud to the 4K cold load. In this case the 4K boundary node was kept fixed, while the 50 K stage temperature was considered oscillating, at 60 s period, with an amplitude of 0.1 K.
The resulting conductive load, through the waveguides, upon the cold load is 5.678 mW. This power shows very stable, because fluctuations are completely damped through the waveguides, while a residual fluctuating radiative power is transferred from the 50 K shroud to the 4 K stage (Figure 13).

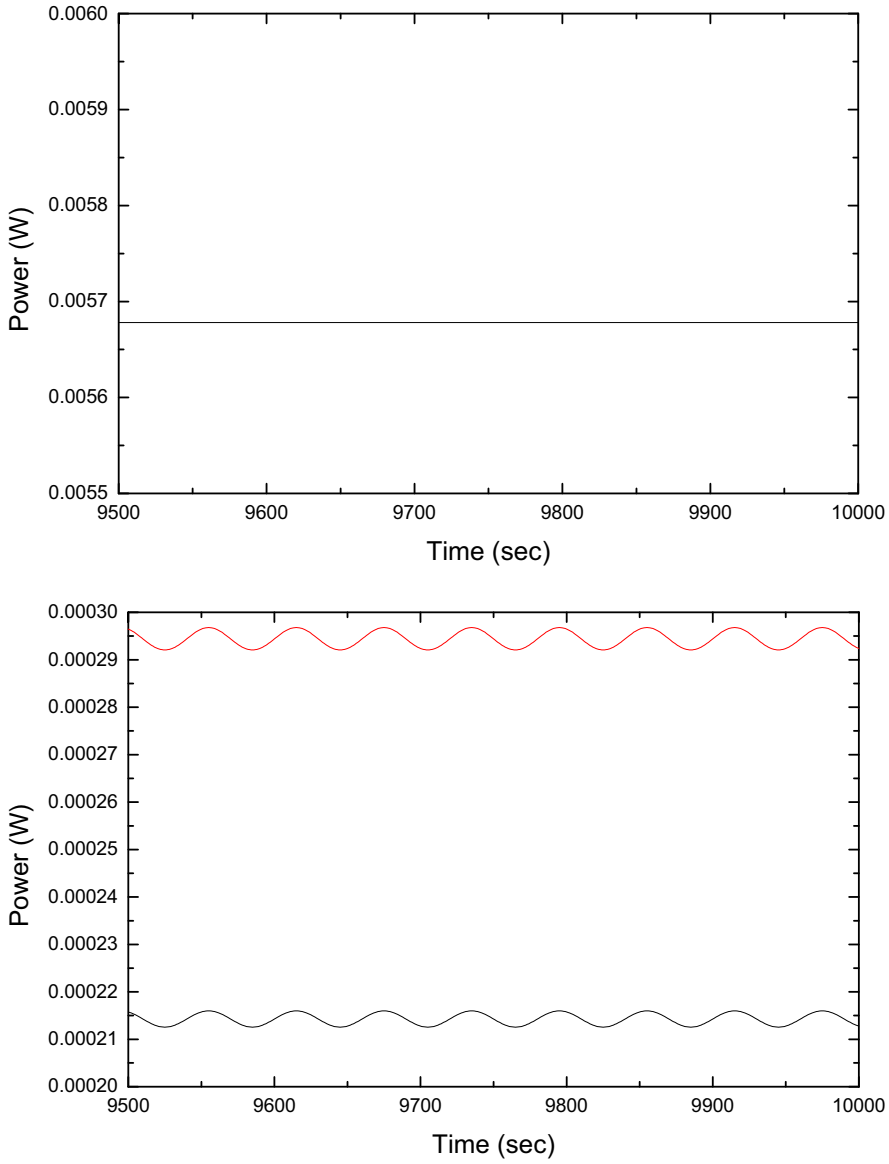

Figure 13 Conductive power transferred through the waveguide upon 4K interface (left panel) and radiative load from 50 K stage to cold load top cover (right panel black curve) and to cold load base (right panel red curve).

7.3 Detailed Fluctuations Analysis

A second set of simulations was performed to evaluate the effect, upon the system, of fluctuations, at the level of the 4 K cooler, with 60 seconds period and 0.1 K amplitude, but with a more detailed representation of the most important section of the calibrator. In fact the Aluminium and pyramid BASE was divided in circular sections, one degree wide with respect to the view angle of the horn.

In Figure 14, some results, which are also useful for the final combined RF and thermal analysis, are reported. In the central part of the bed of pyramids the temperature has risen up to 4.16 K but fluctuations are completely damped (left panel). The temperature at various levels of cylinder internal walls is also shown, outlining the gradual attenuation of the fluctuations (right panel).

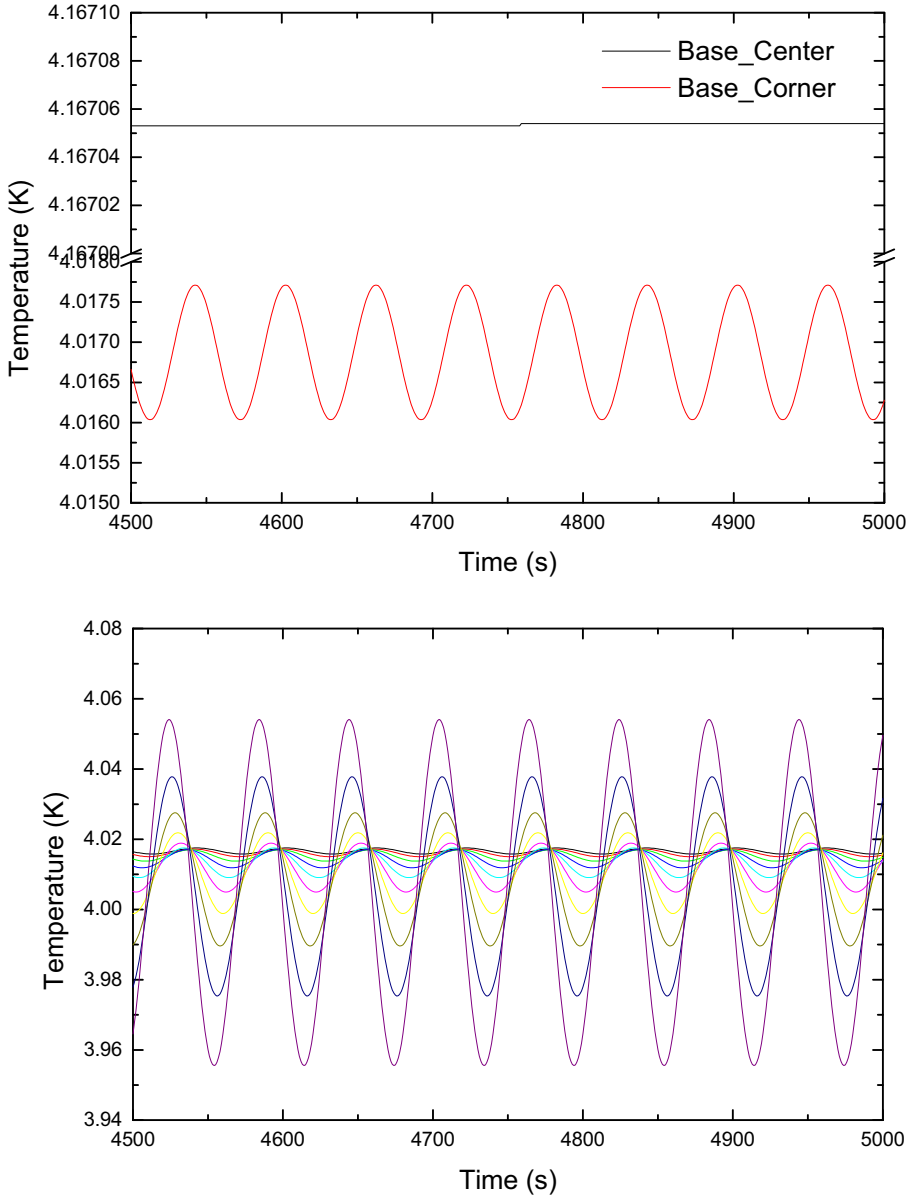

Figure 14 Temperature curves of the pyramid bed center and corner (left panel) and of the cylinder internal wall (right panel)

8 Preliminary Estimate of the Equivalent Temperature

The total power received by the feed horn is the sum of the contributions coming from different parts of the cold load The main features contributing to it are, for each part, *i*, the effective emissivity, ε_i and the physical temperature, T_i. It is then fundamental relating the two characteristics above to describe the environment seen by the feed in terms of a single parameter, which we define as normalised equivalent temperature.

8.1 Method

The internal absorbing surface of the cold load, i.e. the three parts BASE, WALL and LID, has been subdivided in angular sections. The origin of our reference system coincides with the center of the feed mouth; due to the rotational symmetry of the device under study, we can reduce the problem to a two dimensional representation in the plane $\pi[xz]$, where the *x* axis lies on the aperture plane and the z axis coincides with the feed horn axis.
In this frame, the *normalized equivalent temperature* (since the emissivity pattern is normalized to the total power emitted by the feed horn) can be defined as the convolution product of the effective emissivity pattern with the temperature angular distribution. Both the quantities can be expressed in function of the angle θ between the z axis and the vector joining the origin with the middle point of the considered section. So, the entire structure reduces to a discrete succession of elements, each one characterized by a constant (at a specific time) temperature, by its effective emissivity and the angle θ subtended.
Different angular sections have been considered, depending on the part, prioritizing the BASE definition because of its maximum contribute to the total radiometric emissivity (see Tab. 2). Moreover, another, but not less important, criterion to be taken into account is the temperature variation along the different parts: as much as the temperature changes over small angular scales, the number of discrete elements considered increases.
The matching points between two adjacent parts (i.e. BASE-WALL and WALL-LID) are points of singularity for the Ci: we approximate counting only the dominant contribution (the BASE-WALL interface has been counted as the outermost BASE element and the WALL-LID interface as belonging to the WALL).
The BASE was subdivided in annular regions of 1°; the WALL in equal annular regions L/10 mm wide. The LID, in this preliminary study, was considered only as a constant effective emissivity surface, but its contribution to the normalized equivalent temperature is as low as to be neglected in the convolution product (see Tab. 2).

Two models have been studied in this combined method: stationary and transient.

8.2 Stationary model

At first, we evaluated the steady state temperature distribution, assuming the different stages fixed at their nominal temperatures, without any fluctuation. In this case, the convolution of thermal and RF parameters is only dependent by the angular position of the different regions and can be written as:

EQ[18] $$T_{norm} = \int_{\theta} \varepsilon(\theta) \cdot T(\theta) = \int_{\theta} P_r(\theta) \cdot C(\theta) \cdot T(\theta)$$

In the two plots (Figure 15) below, two cases are shown. In the left panel, the normalized equivalent temperature is evaluated for a load with a homogeneous temperature distribution:

EQ[19] $T(\theta) = T_0$

where T_0 is the temperature of the central node of the BASE.
For both the plots, the normalised equivalent temperature is represented as a function of θ, following the relation:

EQ[20] $$\Pi T_{norm}(\theta) = \varepsilon(\theta) \cdot T(\theta) = P_r(\theta) \cdot C(\theta) \cdot T(\theta)$$

In the right panel, the difference between the normalized equivalent temperature pattern evaluated under the approximation in EQ[19] and in the case of a real temperature distribution, is shown.

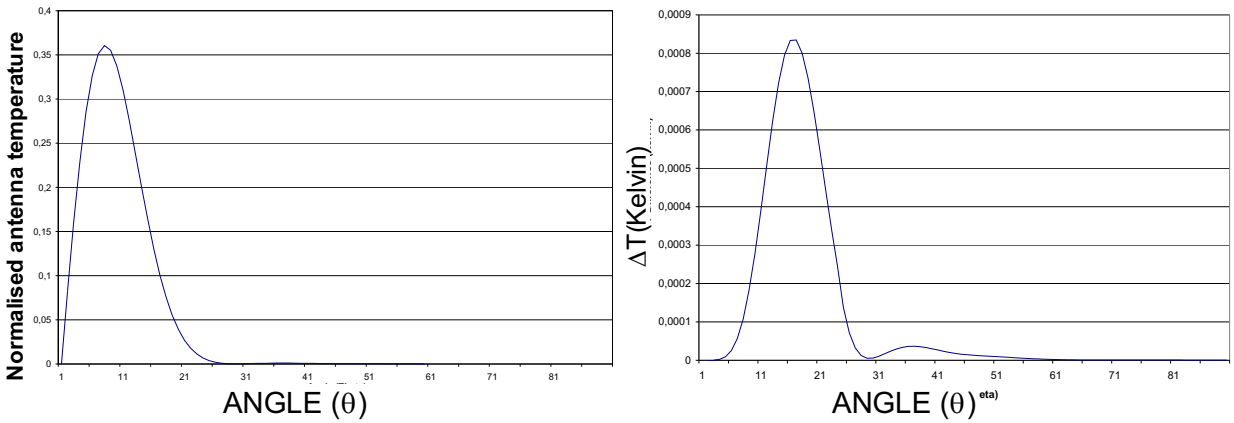

Figure 15 Normalized antenna temperature ΠT(θ): the left pattern is obtained convolving the effective emissivity with a constant temperature distribution, corresponding to that of the BASE central region; the right panel shows the difference with the case obtained considering the full simulated temperature distribution

Integrating the EQ[20] over θ gives the value for T_{norm} (EQ[18]) in both the cases:

EQ[21] $$\left(T_{norm}\right)_{T=const} = 4.162183$$

EQ[22] $$\left(T_{norm}\right)_{T_{distribution}} = 4.152269$$

The two models differ for an amount of 10 mK about in the equivalent temperature measured with a maximum difference $\Delta T_{max} \sim 10$ μK registered in the sector, belonging to the BASE, corresponding to the angle θ = 18°.

8.3 Transient model

Finally the transient case was investigated. Following the same procedures used to analyse the steady state, we have considered the temperature curves reported in Section 7.3, obtaining a time varying equivalent temperature:

EQ[23] $$T_{eq}(t) = \int_{\theta} \varepsilon(\theta) \cdot T(\theta,t) d\theta = \int_{\theta} P_r(\theta) \cdot C(\theta) \cdot T(\theta,t) d\theta$$

In the case considered, the integral is replaced by a series over all the Sky Load sections, individuated by the θ angle. The result is the curve shown in Figure 16.

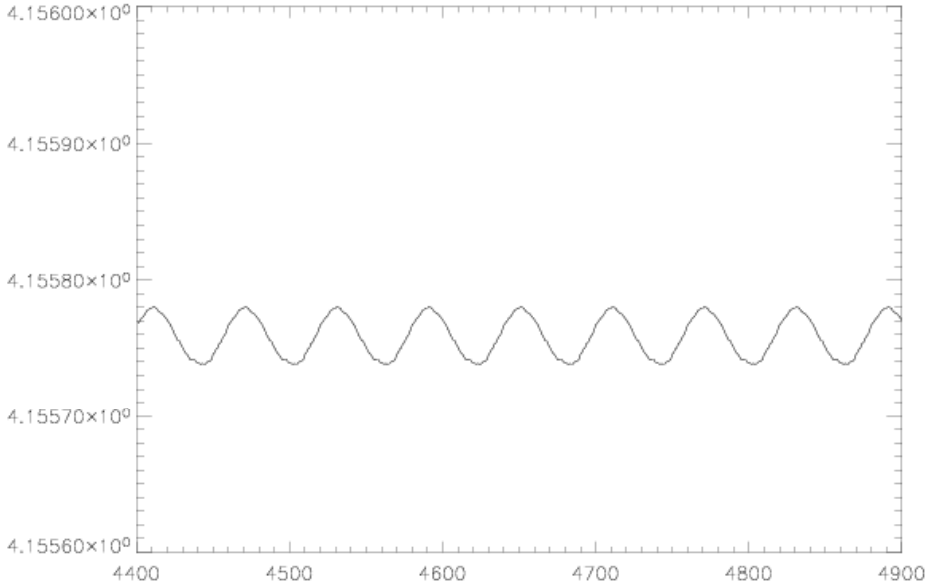

Figure 16 Equivalent temperature (on y axis) fluctuation with time (on x axis) .

As it is evident from the figure, a fluctuation of 0.1 mK of the 4K cooler produces a 40 μK peak-to-peak amplitude fluctuation in the equivalent temperature.
In the Figure 17, the different contributions from BASE and WALL are shown.

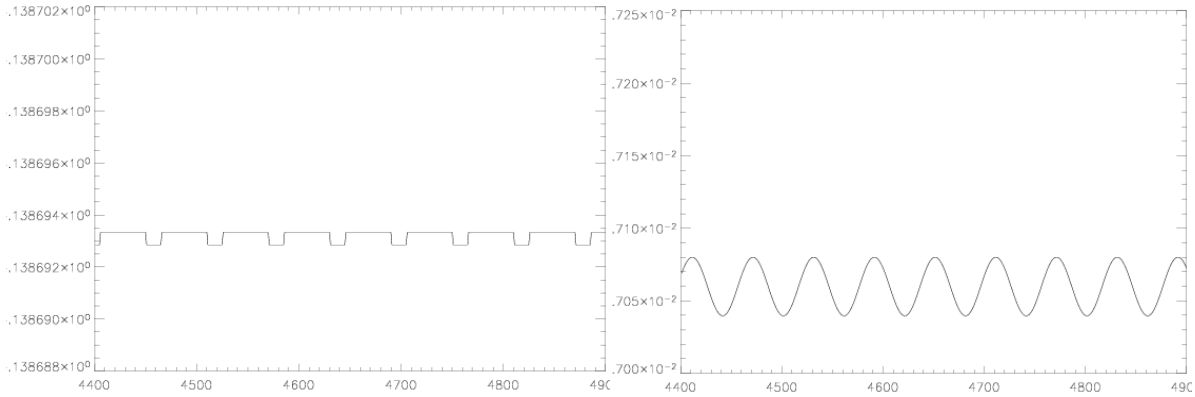

Figure 17 Contribution to total equivalent temperature from BASE (left panel) and WALL (right panel) of the load.

9 CONCLUSIONS

In this note, a cold load for the calibration of the LFI 30 and 44 GHz radiometer chains is presented. In the first part, details about the procedure followed to get a design responding to the main requirement of the calibrator, which is an emissivity higher than 0.997, are shown.
After a description of the cold load design, the analysis of its radiofrequency and thermal behavior is reported.
Finally, we have proposed here a method to investigate in detail the performances of a microwave cold load to be used for a sensitive instrument calibrations. We have shown how radiometric and thermal properties are strictly interconnected to obtain a right understanding of the system at the high level of accuracy we need.
Both steady and transient states have been studied.
In the stationary case, we showed how an error of about 10 mK in the temperature seen by the feed horn is obtained in absence of an accurate physical temperature knowledge. The main contribution to this error is due to temperature inhomogeneity in the BASE.
In the transient study, we found that residual fluctuations in the signal measured is mainly driven by the WALL instability (about 40 μK fluctuation vs. 1 μK in the BASE, see Figure 17), a behavior which could remain hidden by an uncorrelated thermal and RF analysis.

10 References

REF[1] R.E.Bedford and C.K.Ma, *Emissivities of diffuse cavities: Isothermal and nonisothermal cones and cylinders*, J.Opt.Soc.Am.64,3,(1974)

REF[2] C.K.Ma and R.E.Bedford , *Design of an isothermal cavity with nonuniform local intrinsic emissivities to give true blackbody radiant characteristics*, Rev.Sci.Instrum,63 (5),May 1992.

REF[3] M.Halpern , H.P.Gush, E.Wishnow, Vittorio De Cosmo, *Far infrared transmission of dielectrics at cryogenic and room temperatures: glass, Fluorogold, Eccosorb, Stycast, and various plastics,* Applied Optics, vol 25, N°.4, 15 Feb. 1995

REF[4] S. James, W.Lamb, *Miscellaneous data on materials for millimetre and submillimetre optic*s, http://www.ovro.caltech.edu/~lamb/ALMA/Receivers/mmMaterialProperties2.pdf

REF[5] *Application Notes, Emerson & Cuming* Corporation, 1977 http://www.eccosorb.com

REF[6] H.Anzai, M.Saikawa, Y.Naito, T.Mizumoto, *The Equivalent Representation of Pyramidal Absorbers and its Application to the analysis of Electromagnetic Wave Absorber's Characteristics*, IEEE trans. on MMT

REF[7] F. Cuttaia, *RF Comparative analysis of materials and design for Planck Cold Load,* PST-TN-047, August 1st, 2003

REF[8] Seiffert, M., Mennella, A., Burigana, C., et al 2002, A&A, 391, 1185

REF[9] J. C. Mather et al, *Calibrator Design for the COBE Far-Infrared Absolute Spectrophotometer (FIRAS)*, ApJ, 512, 511, 1999

REF[10] F. Cuttaia, '*Simulation of RF performance of Planck cold load*', PL-LFI-PST-RP-005, June 20th,2003